Contemporary Mathematics
Volume **628**, 2014
http://dx.doi.org/10.1090/conm/628/12547

Multi-Bond Models for Platelet Adhesion and Cohesion

Tyler Skorczewski, Boyce E. Griffith, and Aaron L. Fogelson

Abstract. The initial response to blood vessel injury is formation of a platelet aggregate to seal off the damage to the vascular wall. To form the aggregate, platelets adhere to the vascular wall and cohere to one another. Both of these processes involve the interplay of multiple types of receptor-ligand bonds with different force-dependent binding kinetics. The local fluid dynamics affects the bond dynamics by exerting shear stresses on the platelets. We present a mesoscale stochastic binding model based on recent experimental data about platelet receptor-ligand interactions and incorporate it into an immersed-boundary-based platelet aggregation model. Multiple bond types and activation of platelets in response to binding are parts of the model. Simulation results illustrate that the model can capture the stop-start motion of a platelet along the vessel wall as well as the activation-dependent firm adhesion that has been observed experimentally.

1. Introduction

The formation of a platelet plug is the first response to vascular injury. Platelets are small discoid cells which circulate in the blood and whose primary job is to form an aggregate to seal an injury to the vessel wall. In addition to stopping the loss through the injury of cellular elements of the blood (especially red blood cells), platelets in this aggregate provide surface binding sites that support critical coagulation enzyme reactions that ultimately lead to the formation of a fibrin gel that strengthens the initial platelet plug.

For a platelet plug to form, platelets much contact and adhere to the injured vessel wall. That many platelets in the blood are located near the vessel wall to facilitate contact is a result of red-blood-cell-induced platelet margination which leads to concentrations of platelets within a few microns of the vessel wall that are several times the bulk platelet concentration. Platelet margination has been observed in vivo [**31**] and probed experimentally in vitro [**9**, **40**] and the fluid dynamics underlying it has been investigated computationally [**5**, **6**, **44**]. Fluid dynamics, in conjunction with a resting platelet's discoidal shape, further comes into play in determining the motion (e.g., tumbling) of platelet in the near-wall region. Computational studies have looked at near-wall motion of isolated ellipsoidal particles along a flat vessel wall [**28**, **34**], or of elliptical particles in the presence of red blood

2010 *Mathematics Subject Classification.* Primary 65M06, 74F10, 76Z05, 92C35.

cells along a flat vessel wall or near the surface of a prototypical porous thrombus that projects into the vessel lumen [**38**]. These studies suggest that discoidal platelets often first contact the wall along their narrow edge.

When a platelet contacts the damaged vessel wall it may adhere to it. Adhesion occurs through binding of specific receptor molecules on the platelet's surface to specific ligand molecules on the injured vessel wall. It has become increasingly clear that adhesion is a complex process that involves multiple types of receptor-ligand pairs, that the different pairs have different binding/unbinding kinetics, and that it is through the concerted actions of multiple types of receptor-ligand adhesion interactions that a platelet may become firmly attached to the vessel surface [**18**, **27**, **36**]. It is believed that it is the diverse properties of these multiple types of binding pairs that give platelets their remarkable ability to adhere under the full range of flow shear rates (50-2000 s^{-1} physiologically, and much higher pathologically) found in the circulation. Flow is important to platelet adhesion not only in delivering platelets to the near-wall region and in influencing the time they have to react with the vascular surface, but also in influencing the longevity of the adhesive bonds whose unbinding rates are sensitive to the force exerted on them [**1**, **25**, **41**].

Some types of platelet adhesion receptors (importantly, GPIb) are available on a platelet in the unactivated state in which it normally circulates, but others (importantly, the integrin $\alpha_{IIb}\beta_3$) become available only if the platelet has become activated [**19**]. Thus binding between platelet GPIb receptors and von Willebrand factor (vWF) molecules adsorbed to the injured wall can occur without prior priming of the platelet, but bonds between platelet $\alpha_{IIb}\beta_3$ receptors and vessel-surface-bound vWF or fibrinogen molecules do not form until the platelet is activated. Further, the properties of the GPIb-vWF bonds are such that alone they cannot firmly immobilize a platelet to the vessel surface, so firm arrest of a platelet on the injured walls requires additional bonds, often ones between $\alpha_{IIb}\beta_3$ and vWF or fibrinogen. A hypothesized role of the always-available GPIb receptors is to form transient bonds with vWF to slow the platelet's motion along the injured surface in order to give it time to become activated and for its $\alpha_{IIb}\beta_3$ receptors to come into play. Another role for the GPIb-vWF bonds is to provide the platelet with a signal to begin its activation process [**21**]. Physiologically other stimuli, including soluble agonists released by already-activated platelets, and bonds formed between other families of platelet surface receptors and collagen fibers embedded in the injured tissue, provide additional activation stimuli [**24**].

Our earlier models [**10**, **13**] treated the kinetics of platelet adhesion and cohesion binding/unbinding in what is now clearly an overly simple way. Recent experimental studies have provided much new information about the force-dependent unbinding kinetics of the bonds involved in platelet [**1**, **7**] and other blood cell (e.g., leukocyte) adhesion [**3**, **42**]. In particular, the evidence suggests that a bond between $\alpha_{IIb}\beta_3$ and fibrinogen breaks at a rate that increases with the force acting on it (so-called 'slip bond' behavior) while a GPIb-vWF bond displays more complex 'catch/slip bond' behavior, in which its unbinding rate decreases with increasing force over a range of applied forces and then increases if the force is further increased [**1**, **32**, **41**].

In this paper, we use this new information to develop a mesoscale model for the binding/unbinding kinetics of two types of platelet bonds; GPIb with vWF and $\alpha_{IIb}\beta_3$ with its ligands. We combine this model with the immersed boundary

method to compute the fluid-structure interactions that occur during platelet adhesion and cohesion under flow. We also account for platelet activation triggered by GPIb-vWF bond formation and for the activation-induced upregulation of the $\alpha_{IIb}\beta_3$ receptors. Our binding model is mesoscale in that, rather than tracking the state of every receptor and ligand as bonds are stochastically formed and broken as well as calculating a force for each receptor-ligand bond, it uses an elastic link emanating from a platelet immersed boundary point to represent an integer number of bonds. That number varies as bonds are stochastically formed or broken and the stiffness of the link reflects the number of bonds in currently represents. The work we report here is one of a few recent efforts to incorporate up-to-date binding information with fluid-structure interactions in a computational model of blood cell adhesion [**20**, **29**, **30**]. Our work is distiguished from the other work in using the immersed boundary method for the fluid-structure interactions and/or in using a new mesoscale stochastic model for the binding dynamics.

2. Immersed Boundary Method

The immersed boundary (IB) method was first developed by Peskin to study cardiac fluid dynamics [**33**] and has since been expanded to investigate many fluid-structure phenomena including blood flows with red blood cells and platelets [**5**, **6**, **12**, **38**]. The method is concerned with the problem of determining the coupled motions of a viscous incompressible fluid and one or more deformable elastic objects that are in contact with it. Neither the fluid nor object motion is prescribed, rather they influence each other and are determined together.

The IB method uses an Eulerian description of the fluid in terms of its velocity $\mathbf{u}(\mathbf{x},t)$ and pressure $p(\mathbf{x},t)$ at each spatial location $\mathbf{x} \in \Omega$ at time t. It uses a Lagrangian description of each IB object and tracks the location as functions of t, $\mathbf{X}_i(q,t)$, of the point on IB object i labeled by parameter value $q \in \Gamma_i$. The IB equations of motion are

$$\rho\left(\mathbf{u}_t + \mathbf{u}\cdot\nabla\mathbf{u}\right) = -\nabla p + \mu\Delta\mathbf{u} + \mathbf{f}, \qquad \nabla\cdot\mathbf{u} = 0, \tag{2.1}$$

$$\mathbf{F}_i(q,t) = \mathcal{F}_i(\mathbf{X}_i(q,t),t), \tag{2.2}$$

$$\mathbf{f}(\mathbf{x},t) = \sum_i \int_{\Gamma_i} \mathbf{F}_i(q,t)\delta(\mathbf{x}-\mathbf{X}_i(q,t))dq, \tag{2.3}$$

$$\frac{d\mathbf{X}_i}{dt}(q,t) = \mathbf{u}(\mathbf{X}_i(q,t),t) \equiv \int_\Omega \mathbf{u}(\mathbf{x},t)\delta(\mathbf{x}-\mathbf{X}_i(q,t))d\mathbf{x}. \tag{2.4}$$

Equations 2.1 are the Navier-Stokes equations for a fluid with constant density ρ and viscosity μ and subject to a driving force density $\mathbf{f}$, and hold at all points of the domain. Equation 2.2 represents a recipe for calculating a force density (per unit q) at points of the IB objects consistent with the mechanical properties it is desired those objects have. Equation 2.3 defines the fluid force density $\mathbf{f}$ in terms of the immersed boundary elastic force densities $\mathbf{F}_i$. By integrating both sides of this equation over an arbitrary region of the fluid, we see that the total fluid force on this region equals the total elastic force along the portions of the immersed boundaries, if any, that pass through this region. Hence nonzero values of the fluid force density occur only at spatial points that coincide with an IB point. Finally, Equation 2.4 specifies that the velocity of each IB point is the same as that

of the fluid at the same location. This is a statement that the no-slip boundary condition appropriate for a viscous fluid is assumed to hold along each immersed boundary, but the condition is used in this situation to give the velocity at which the IB point moves. Both Equation 2.3 and 2.4 involve an integral operator that is used to communicate information between the Eulerian and Lagrangian coordinate descriptions. The integral operators for spreading the forces and for interpolating the velocities are adjoints, and this has important implications for the IB method's performance [**33**].

In actual IB calculations, the Navier-Stokes equations are approximated at points of a Cartesian grid placed over the fluid domain Ω. A separate grid of Lagrangian points is used to discretize each IB object, the integrals in Equations 2.3 and 2.4 are replaced by sums over the IB points and the fluid grid respectively, and the δ-function in these equations is approximated by a smooth but very localized function. This implies that the fluid force density is non-zero only for fluid grid points close to the immersed boundaries and that the velocity of each IB point is computed as a weighted-average of the fluid velocity at grid points near the IB point.

In the studies described in this paper, platelets are modeled as fluid-filled ellipses in two dimensions or ellipsoids in three dimensions. The platelet's major axis (axes) is 3.6 μm and its minor axis is 1.2 μm. In order to approximately maintain the elliptical shape of the platelets in our simulations without using very stiff bending forces, we developed a two-layer model of the platelet. The platelet surface, which represents the real platelet's membrane and submembrane cortex, is represented (in 3D) by a triangular mesh of points joined to one another by springs along the triangles' edges. A second layer of points with the same triangulation is located a short distance inside of the surface layer. Points within this layer are joined to one another by springs as in the surface layer. In addition, each IB point in the inner layer is connected by a spring to its corresponding point in the surface layer as well as to the points corresponding to its neighbors. A similar strategy is used in the two-dimensional simulations. The cross-linked network of points that results is illustrated in Figure 1. All of the springs connected to a platelet IB point contribute to the IB force $\mathbf{F}$ at that point. The numerical parameters used in the simulations are listed in Table 1.

In addition to the forces generated by the springs used in representing each platelet, other forces may be generated by 'links' used to model adhesion of a platelet to the vessel surface or cohesion of two platelets to one another. Adhesive and cohesive links form and break during a simulation according to dynamical rules described below. Each adhesive link connects a platelet IB point to a point on the vessel wall, and each cohesive link connects IB points on distinct platelets. Each link may represent multiple biological bonds and the force generated by the link depends on its length, on the numbers and types of bonds it represents, and on their prescribed mechanical properties. For a platelet IB point that is the terminus of a link, the link force contributes to the total IB force at that point.

2.1. Adaptive Mesh Refinement. In order to achieve high spatial resolution near the platelets we employ adaptive mesh refinement (AMR) near IB points. In our AMR scheme we divide the Eulerian Cartesian grid into two levels each representing a different level of refinement. Level 0 represents the coarsest level

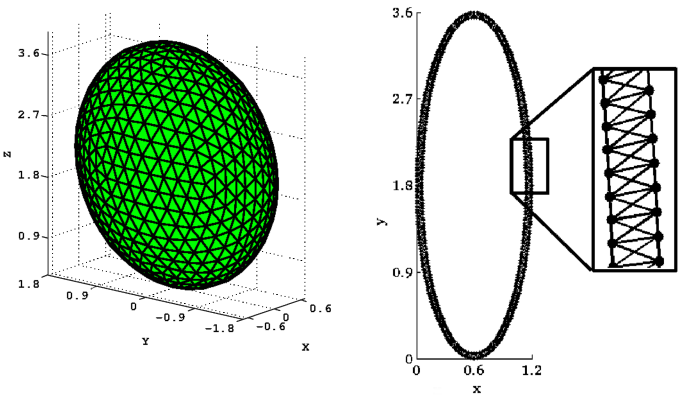

FIGURE 1. 3D and 2D platelets used in this study. Scale is microns. Lines represent stiff springs.

TABLE 1. Simulation parameters

number of IB points per 3D platelet	5124
number of IB points per 2D platelet	512
platelet major axis	3.6 μm
platelet minor axis	1.2 μm
domain dimensions	$20 \times 6 \times 10$ μm
Δx coarse	93.75 nm
Δt	8e-8 sec

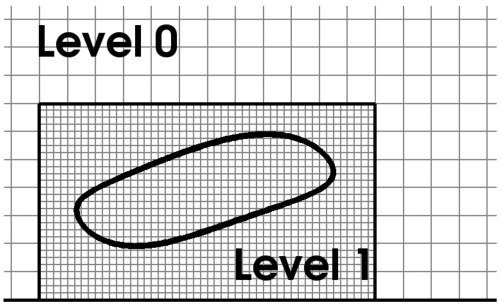

FIGURE 2. Adaptive Mesh Refinement (AMR) scheme

and refinement increases by a factor of four as the level index increases. See Figure 2. Each level is divided into several computational patches which facilitates domain decomposition for parallel computation. This scheme is implemented in the IBAMR code developed by Griffith [**14**]. To use IBAMR for this project, we extended it to allow dynamic creation and removal of links between IB points,

3. Force required to immobilize platelet

We first use the IB method to calculate the force required to immobilize a platelet attached to the vessel wall in a shear flow. Analytical results of this type

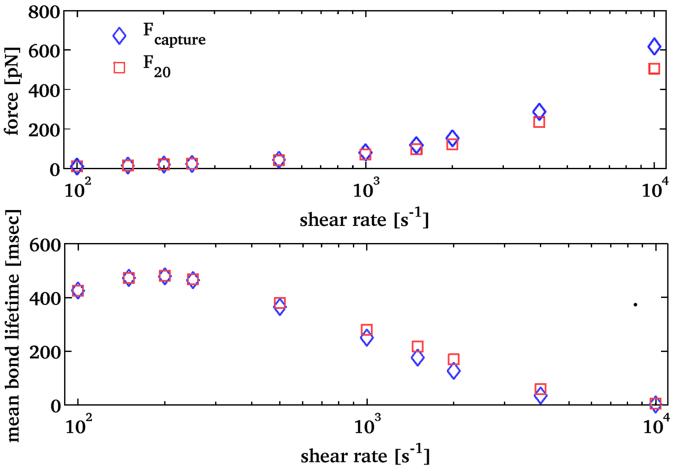

FIGURE 3. (top) Force required for a single unbreakable bond to immobilize a 3D platelet against shear rate. (bottom) Mean lifetime of such a bond when the force calculated is plugged into off rate model given by equation 4.1. Maximum forces experienced by the bond and calculated mean bond lifetimes over the course of a 20 msec simulation are shown with blue diamonds and bond forces and calculated mean lifetimes at equilibrium are shown with red squares.

are available for spherical particles, but seem not to be available for ellipsoidal and similarly-shaped objects. The simulation begins with a platelet oriented perpendicular to the vessel surface and connected to it by a simple spring (stiffness 10 pN/nm and rest length 50 nm) initially at its rest length. The flow is driven by moving the top wall at a prescribed speed in the x-direction. In the simulation the spring is not allowed to break, and the platelet tips over and comes to rest.

Over the course of this motion, the spring stretches to a maximal length and then retracts as the platelet becomes more aligned with the vessel wall. The platelet-spring system reaches equilibrium in less than 20 msec. We measure the force on the spring during this motion. We call the maximum force exerted on the spring the 'capture force' since a bond would have to withstand this force in order to survive long enough to immobilize the platelet. In Figure 3-top we show this force as well as the force at 20 msec required to hold the platelet at equilibrium for each of a number of shear rates. The magnitude of the force varies from 15.6 pN at shear rate 150 s^{-1} to 618 pN at shear rate 10,000 s^{-1}.

4. Early platelet-vessel wall adhesion with GPIb-vWF bonds

The platelet surface bears at least four types of receptors involved in platelet adhesion to the vessel wall. There are approximately 25,000 GPIb receptors which can bind to the protein vWF adsorbed on the vessel wall. There are 50,000 to 80,000 $\alpha_{IIb}\beta_3$ integrin receptors which can bind to vWF as well as other proteins, notably fibrinogen, that have adsorbed to the vessel wall [**35**]. There are approximately 1000-2000 each of GPVI and $\alpha_2\beta_1$ receptors that can bind directly to collagen

fibers on the subendothelial matrix exposed by an injury to the vessel wall. All four types of receptors are involved to some degree in the mechanics of adhesion and generating intraplatelet biological signals. However, at moderate and high shear, the GPIb and $\alpha_{IIb}\beta_3$ receptors appear to be the primary ones responsible for slowing and arresting platelet motion and are the subject of the modeling that follows. Key differences between these two receptors are that GPIb receptors operate on a fast timescale and can act right away while $\alpha_{IIb}\beta_3$ receptors require activation before they can play a significant role in the adhesion process and they operate on a slower timescale. We first focus on unactivated platelets and GPIb receptors. Later we introduce a simple model of platelet activation and consider adhesion mediated by both GPIb and $\alpha_{IIb}\beta_3$ receptors. Many models of binding dynamics track the number of bonds, n, between two surfaces with an equation of the form

$$\frac{dn}{dt} = k^+(n_{max} - n) - k^- n,$$

or a stochastic analog of it [**23**]. Here n_{max} is the maximum number of bonds, k^+ is the rate per available receptor at which bonds form and k^- is the rate per bond at which bonds break. We use an equation of this form for each of two populations of bonds, the 'fast' GPIb-vWF bonds and the 'slow' $\alpha_{IIb}\beta_3$-mediated ones. Quantities related to the fast (slow) bonds are indicated by subscript f (s).

4.1. GPIb-vWF unbinding. It is becoming increasingly clear that bonds between GPIb and vWF exhibit catch and slip bond dynamics for different force regimes. A catch bond is one for which the unbinding rate decreases as the force applied to the bond increases, while for a slip bond the unbinding rate increases with increasing applied force. The GPIb-vWF bonds behave as catch bonds for forces below a critical level and as slip bonds for larger forces. This behavior is believed to stem from the existence of multiple conformations of the vWF molecule and the fact that changes between the conformations are force-dependent.

Following Auton et al. [**1**], we assume vWF can exist in two conformational states, a native state (N) and a stretched 'intermediate' state (I). When the vWF molecule of a GPIb-vWF bond is in the N state, the mean bond lifetime increases with increasing applied force. That is, the bond behaves as a catch bond. When the vWF is in the I state, the bond behaves as a slip bond, with the mean bond lifetime decreasing with increasing applied force. Because vWF transitions between N and I states at rates that also depend on applied force, the GPIb-vWF bond exhibits 'catch-slip' behavior. As in [**1**], we take the off-rate of the GPIb-vWF bonds, k_f^-, to be given by

$$k_f^- = \frac{1}{1+\kappa^0} k_N e^{S_f(L-L_0)y_N/k_BT} + \frac{\kappa^0}{1+\kappa^0} k_I e^{S_f(L-L_0)y_I/k_BT} \tag{4.1}$$

where κ^0 is given by

$$\kappa^0 = k_T e^{S_f(L-L_0)y_T/k_BT}. \tag{4.2}$$

In Equation 4.1, the Bell-model-type [**2**], terms

$$k_N e^{S_f(L-L_0)y_N/k_BT} \text{ and } k_I e^{S_f(L-L_0)y_I/k_BT}$$

are the unbinding rate expressions for a GPIb-vWF bond 'locked' in the N or I state, respectively. In these expressions, S_f and L_0 are the bond stiffness and rest length, respectively, and k_N and k_I are the rates of unbinding from the N and I

TABLE 2. GPIb-vWF bond model dynamics parameters [**1**]

parameter	symbol	value
GPIb-vWF bond stiffness	S_f	10 pN/nm
N-state vWF unloaded bond breaking rate	k_N	4.9 s^{-1}
N-state vWF compliance factor	y_N	-0.23 nm
I-state vWF unloaded bond breaking rate	k_I	1.84 s^{-1}
I-state vWF compliance factor	y_I	0.039 nm
unloaded vWF state partition term	k_T	0.4
vWF state partition compliance factor	y_T	0.45 nm
thermal energy	k_BT	4.1 pNnm

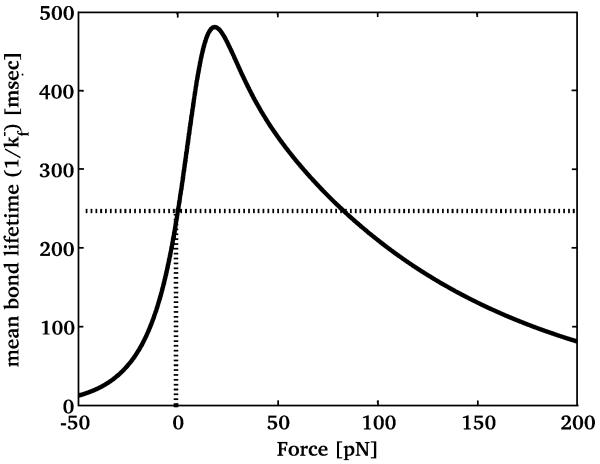

FIGURE 4. bond lifetimes vs force. We see that for low forces the mean bond lifetime is an increasing function of force - indicating a catch bond. The unloaded mean lifetime is 248.8 msec. The mean lifetime peaks at 480.5 msec when the force is 18 pN and decreases for forces greater than 18 pN - indicating slip bond kinetics.

states, respectively, when the bond is unloaded. Because $y_N < 0$ and $y_I > 0$ the rate of unbinding from the N state decreases and that from the I state increases as the bond is stretched. The fact that the vWF molecule can transition between N and I states is captured in κ^0. The expression $\frac{1}{1+\kappa^0}$ is the probability that a GPIb-vWF bond of length L is in state N and $\frac{\kappa^0}{1+\kappa^0}$ is the probability it is in state I. These probabilities change with respect to the force applied to the bond. Because $y_T > 0$, κ^0 increases with applied force, leading to an increased probability of slip-bond behavior.

Table 2 shows the values of the various parameters of the model. Figure 4 shows the mean bond lifetime, calculated as $1/k_f^-$, against force for these parameter values. Note that bond lifetimes are increased compared to unloaded bond lifetimes for forces from 0 pN to 82 pN and that compressive forces lead to substantially shorter lifetimes.

Using this model and the results above relating force to bond lifetimes we can then predict how long a single bond bearing the force required to immobilize

a platelet will survive. In Figure 3-bottom we plot mean lifetime versus shear rate. The lifetime results display a biphasic behavior typical of catch to slip bond dynamics. For shear rates less than 200 s^{-1} the mean bond lifetime increases with increasing shear rate. Above 200 s^{-1} the mean bond lifetime decreases with increasing shear rate.

4.2. GPIb-vWF binding. GPIb receptors on the platelet bind to the A1 domain on vWF proteins [**17**]. vWF is a multimeric protein that ranges in length from 100 nm up to 1 micron or more and can have numerous A1 domains along its length [**39**]. Thus, the distance from a wall at which the platelet encounters an A1 domain on vWF can vary substantially.

We model the GPIb-vWF binding rate as depending on the distance between the receptor and the wall. More specifically, we assume that the distance from the wall that a vWF protein extends has a probability density function $f(y)$, where y is the distance from the wall. Should a GPIb receptor be closer to the vessel wall than the distance a vWF protein extends from the wall, we assume the GPIb receptor contacts all A1 domains on the overlap portion of the vWF protein. Thus, integrating this pdf function from y to ∞ gives the probability $P(y)$ a GPIb receptor at a distance y from the vessel wall encounters a VWF A1 domain. For this study we use the fact that the mean length of vWF in its extended state is 350 nm [**39**] and assume a normal distribution with standard x deviation of 100 nm to define the pdf $f(y)$:

$$P(y) = \int_y^\infty f(y)dy, \tag{4.3}$$

where,

$$f(y) = \frac{1}{\sqrt{2\sigma}} e^{\frac{(y-\bar{y})^2}{\sigma^2}} \tag{4.4}$$

With this information and denoting by k_f^+ the rate of binding between an A1 domain and an available GPIb receptor we have the rate of bond formation

$$k_f^+ P(y)\,(n_{fmax} - n_f) \tag{4.5}$$

Here n_f represents the number of GPIb-vWF bonds, and $(n_{fmax} - n_f)$ is the number of GPIb receptors minus the number used in GPIb-vWF bonds and represents the number of available receptors.

4.3. Qualitative behavior of a cartoon continuum model. Before carrying out full IB simulations of platelet adhesion that involve these binding models, it is illuminating to look at a simplified model of this process. Let us assume for now that n_f takes values in $[0, n_{fmax}]$.

The net time rate of change of n_f is described by

$$\frac{dn_f}{dt} = k_f^+ P(y)\,(n_{fmax} - n_f) - n_f k_f^-(L) \tag{4.6}$$

where we note that the off rate depends explicitly on the length of the bond (L).

We focus on the time immediately after a platelet first becomes sufficiently close to the injured wall to bind to it. We assume a link forms, and use $L(t)$ to denote its length and $n_f(t)$ to denote the number of bonds represented by the link. We observe from the computations used to determine the force required to immobilize a platelet that the time rate of change of the link length is an approximately linear

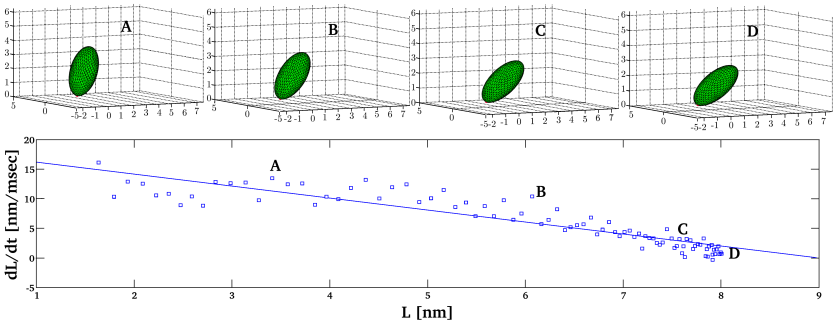

FIGURE 5. (Top) Snapshots from a simulation like that described in Section 3. (Bottom) Measurements of $\frac{dL}{dt}$ vs. link length L from the simulation.

function of link length. See Figure 5. Thus, we model the time rate of change of link length as a linear function of L, where the link length grows at a rate proportional to the shear rate and contracts at a rate proportional to the bond number and the link length.

$$\frac{dn_f}{dt} = k_f^+ 0.5\,(n_{fmax} - n_f) - n_f k_f^- \tag{4.7}$$

$$\frac{dL}{dt} = \beta\gamma - cS_f n_f L \tag{4.8}$$

where

$$k_f^- = \frac{1}{1+\kappa^0} k_N e^{S_f L y_N/k_B T} + \frac{\kappa^0}{1+\kappa^0} k_I e^{S_f L y_I/k_B T} \text{ and } \kappa^0 = k_T e^{S_f L y_T/k_B T}.$$

Note that we have set $P(y) = 0.5$ in Equation 4.5 to obtain Equation 4.7 and have set the bond rest length to zero. In Equation 4.8, c is a constant of proportionality derived from Stoke's drag law.

For an equilibrium state (n_f^*, L^*) of Equations 4.7-4.8

$$L^* = \beta\gamma/cS_f n_f^* \tag{4.9}$$

and

$$0.5k_f^+ \left(n_{fmax} - n_f^*\right) = n_f^* \left(\frac{1}{1+\kappa^0} k_N e^{S_f L^* y_N/k_B T} + \frac{\kappa^0}{1+\kappa^0} k_I e^{S_f L^* y_I/k_B T}\right) \tag{4.10}$$

Using 4.9 in 4.10 yields a transcendental equation for n_f^* which has up to two solutions depending on parameter values.

Consider the effect of varying the bond formation rate k_f^+. Analyzing the transcendental equation, we see that there is a critical value, $k_{f,critical}^+$, such that for $k_f^+ < k_{f,critical}^+$ there is no equilibrium, for $k_f^+ = k_{f,critical}^+$ there is one equilibrium solution, and for $k_f^+ > k_{f,critical}^+$ there are two equilibria. In the last situation, the equilibrium with the smaller n_f value is a saddle node and the other equilibrium is a stable node.

If there are no equilibria in the system, we observe that the long-time asymptotic state of the system tends towards one with no bonds and an infinite link length, indicating that the platelet is no longer adhered to the wall. If there are

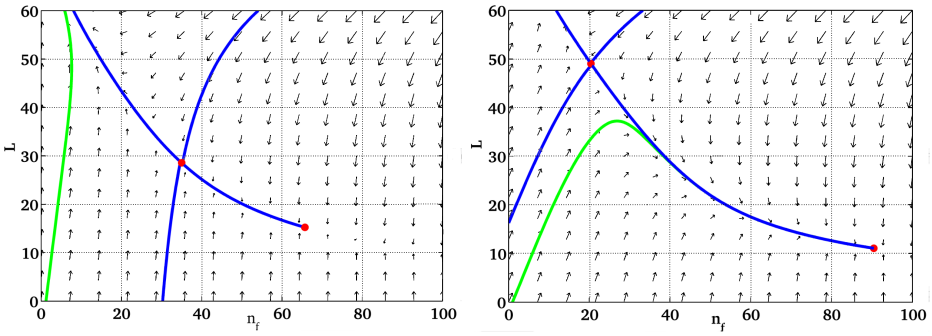

FIGURE 6. Phase plane with fixed points of reduced system. The left fixed point is a saddle point and stable/unstable manifolds are shown in blue. Green curves show the trajectory of an adhesive link with one bond formed at rest. Note the magnitude of the stochastic nature of the system means the actual dynamics could be jumping across these lines. The right fixed point is a stable node. The left phase plane shows the dynamics of a system that has a value of k_f^+ such that a bond formed at rest will initially feel an increased pressure to add bonds but will ultimately detach. The right phase plane has an increased k_f^+ where the initial conditions of a single bond formed at rest ultimately leads to stable adhesion.

two equilibria, the state space is separated into two regions by the stable manifold of the saddle point. One region has solutions which tend to the stable node, i.e. a stably adhered platelet, and the other region contains solutions which ultimately lead to an unadhered platelet. Note that for platelets starting in this region with a low bond number and small link length, the dynamics of the system are to initially add bonds before breaking them.

Another interesting transition occurs as k_f^+ is increased starting from a value slightly greater than $k_{f,critical}^+$. The point $(n_f = 1, L = 0)$ starts outside of the basin of attraction for the stable equilibrium point, but enters it as k_f^+ is increased. This implies that for k_f^+ sufficiently large, a single bond formed under no loading ultimately leads to stable platelet adhesion. See Figure 6.

While we investigate how changing k_f^+ affects the system dynamics because this parameter is unknown, investigating the system behavior for different shear rates (and with a fixed k_f^+) can provide information on platelet adhesion in various physiological regimes. Figure 7 shows the equilibrium solutions to Equation 4.10 for a fixed k_f^+ and several different shear rate values. As the shear rate decreases we see the same qualitative behavior as when increasing the value of k_f^+. For large values of the shear rate there are no equilibria. As the value decreases to a critical value there is one equilibrium solution and if decreased further there are two equilibria. These results suggest that for a single family of bonds with the kinetics as described, there is a maximum shear rate beyond which stable long-term adhesion is not possible.

4.4. Platelet adhesion simulation. We next turn to two-dimensional IB-based simulations of platelet adhesion that incorporate stochastic analogs of the

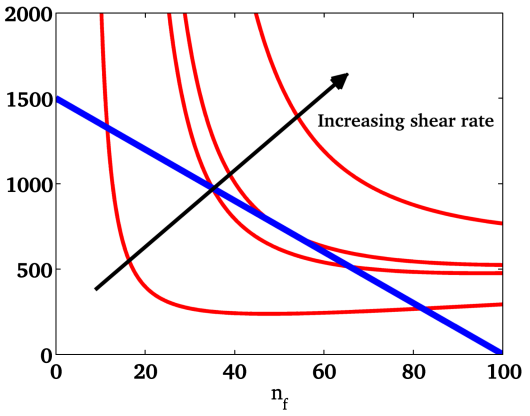

FIGURE 7. Intersections between the blue curve (bond formation) and red curves (bond breaking) identify solutions to the transcendental equation 4.10 for shear rate values 500, 1000, 1100 and 1500 s^{-1}. For these curves $k_f^+ = 30$, $\beta/cS_f = 1$ and other parameters are given in Table 2. As the shear rate decreases we see that we go from no equilibrium solutions to one at a critical shear rate to two equilibrium solutions.

binding and unbinding models described above. The domain is a channel whose bottom wall is reactive and whose top wall is moved with a prescribed velocity to generate a background linear shear flow. A platelet is placed close to the reactive wall. We allow an adhesive link to form between any IB point on the platelet's outer layer and any point on the reactive wall. A link to a platelet IB point is formed stochastically with a probability given by Equation 4.5 with $n_f = 0$. The resulting link connects that IB point to the point on the wall to which it is closest at the time the link forms. For each existing link, we track the integer number n_f of GPIb-vWF bonds that it represents. At the time the link forms n_f is set to 1, n_f can reach a maximum of n_{fmax}, and if a link's bond number drops to zero, the link is removed. In each timestep, the bond number is incremented by 1 with probability $1 - exp(\Delta t k_f^+ P(y)(n_{fmax} - n_f))$ where Δt is the timestep and the rate of bond formation comes from Equation 4.5. The bond number is decremented by 1 with probability $1 - exp(\Delta t n_f k_f^-)$. Thus, we are updating the bond number under the assumption that binding and unbinding are distinct Poisson processes with the parameters indicated, and that Δt is sufficiently small that only one event of each type can occur per timestep. If a link represents multiple bonds, we set its rest length L_0 to be the average of the link lengths at the times at which each of the bonds formed. A link generates a force at the IB point that points in the direction of the link and has magnitude

$$F = n_f S_f (L - L_0).$$

During each timestep of our simulation proceeds as follows

(1) For each IB point, update bond numbers stochastically through the dynamics presented in Equations 4.1 and 4.5.

(2) Using this bond information and the configuration of the IB points, calculate, the forces $\mathbf{F}(X,t)$ at each IB point.
(3) Spread these forces to the Eulerian grid with a discrete form of the spreading operator given in Equation 2.3.
(4) Solve a discrete form of the Navier-Stokes equations (Equations 2.1) to determine the new velocity field.
(5) Using the computed velocity field interpolate the velocity from the Eulerian grid to the IB points using a discrete form of Equation 2.4.
(6) Update the positions of the IB points using these interpolated velocities.

To investigate how these models of bond formation and breaking affect the dynamics of platelet adhesion, we performed several series of two-dimensional simulations. The platelet is represented by IB points using the two-layer arrangement discussed previously. Only IB points on the outer layer can form links with the vessel wall.

4.5. Simulation Results. We first performed an experiment to determine the force required to immobilize a two-dimensional platelet attached irreversibly to the wall. This is analogous to the three-dimensional simulations discussed in Section 3. For the current simulation, the top channel wall was moved to drive a flow with shear rate 2000 s^{-1}, and the single link stretched 39.4 nm for spring stiffness $S_f = 10$ pN/nm, corresponding to a total fluid force on the platelet of 394 pN. At this level of force, the GPIb-vWF unbinding rate formula, Equation 4.1, predicts a mean time of attachment of 12.8 msec. This result suggests that over the course of 100 msec we should expect to see several platelet binding and unbinding events. Thus the simulations we describe next were run for 100 msec.

In each of these simulations, the platelet was initially oriented orthogonal to the wall and it was attached to the wall by a single GPIb-vWF bond. We carried out twelve such simulations for each of three bond formation rates $k_f^+ = 0.15$, 0.25, 0.35 s^{-1}. Values of k_f^+ much greater or smaller than these produce immediately firmly adhering platelets or no platelet adhesion, respectively, behaviors which are not observed experimentally.

We observe four types of behavior across all simulations. The platelet either (1) remains adhered to the vessel wall near its initial point of attachment, or (2) it translates ('slides') along the vessel wall while maintaining at least one bond with the wall, or (3) it slides along the wall in a stop-start fashion with periods of attachment and detachment, or (4) it detaches early in the simulation and tumbles in the shear flow without reattaching. See Figure 8 for an illustration of one such simulation. In these simulations, the platelet detaches early and remains unattached in 83.3 percent of the $k_f^+ = 0.15/s$ cases, 16.6 percent of the $k_f^+ = 0.25/s$ cases, and 8.3 percent of the $k_f^+ = 0.35/s$ cases.

The mean horizontal velocity of the platelet's center of mass was 9.3 μm/s for $k_f^+ = 0.25/s$ and 4.7 μm/s for $k_f^+ = 0.35/s$. For $k_f^+ = 0.15/s$, there were too few events to make a calculation meaningful. These velocities should be compared to one of 1200 μm/s at a distance of one platelet minor radius (0.6 μm) from the wall in the absence of the platelet. Figure 9 gives statistics for the bond numbers from these three sets of simulations. We see that, after 100 msec, the mean number of bonds on the platelet for the $k_f^+ = 0.35/s$ case is more than a standard deviation

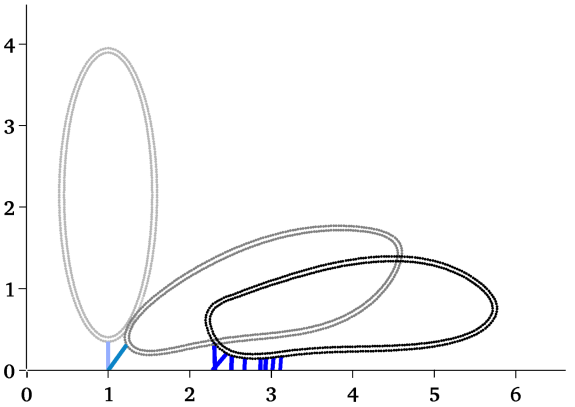

FIGURE 8. Snapshots in time of a platelet initially binding to the vessel wall, tipping over, detaching and reattaching downstream. This detaching and reattaching repeats as the simulation progresses.

above the mean number for the $k_f^+ = 0.25/s$ case. A similar relation holds between the $k_f^+ = 0.25/s$ and $k_f^+ = 0.15/s$ cases.

Figure 10 shows a histogram of bond lifetimes in these simulations. We see that for the higher k_f^+ cases more bonds were produced, as expected. However, we also see that the vast majority of these bonds are very short-lived. The mean bond lifetimes are 5.1, 5.2, and 4.2 msec for the $k_f^+ = 0.15/s$, $k_f^+ = 0.25/s$, and $k_f^+ = 0.35/s$ cases, respectively. Note that these mean lifetimes are significantly shorter than that in the holding experiment described above. It is also interesting to note, see Figure 10, that the $k_f^+ = 0.25/s$ case produced the most very long-lived bonds (lifetimes greater than 60 msec).

Upon further investigation of bond lifetimes in these simulations, we found that most of the short-lived bonds broke when they were under compression. This is a manifestation of the catch-bond mechanism of GPIb-vWF dynamics. Of all of the bonds formed in the $k_f^+ = 0.15/s$ simulations, only 17 of the 173 broken bonds broke when the bonds were stretched beyond their restlength. Similar behavior was seen for the k_f^+ values (24 of 879 for $k_f^+ = 0.25/s$, 23 of 1797 for $k_f^+ = 0.35/s$). That most bonds broke under compression explains the short mean bond lifetimes in these simulations compared to that in the holding experiment. If we restrict our attention to those bonds that broke when stretched, we observe mean lifetimes of 9.3, 27.7 and 27.8 msec $k_f^+ = 0.15/s$, $k_f^+ = 0.25/s$, and $k_f^+ = 0.35/s$ cases, respectively. For the $k_f^+ = 0.25/s$ and $k_f^+ = 0.35/s$ cases, this is more than double the lifetime predicted by the holding experiment. Another interesting point is that while the number of long-lived bonds in the stretched state is fairly consistent across the values of k_f^+, the fractions of platelets which detached are very different. This suggests that the many short-lived bonds that form for higher k_f^+ serve some stabilizing purpose with respect to platelet adhesion.

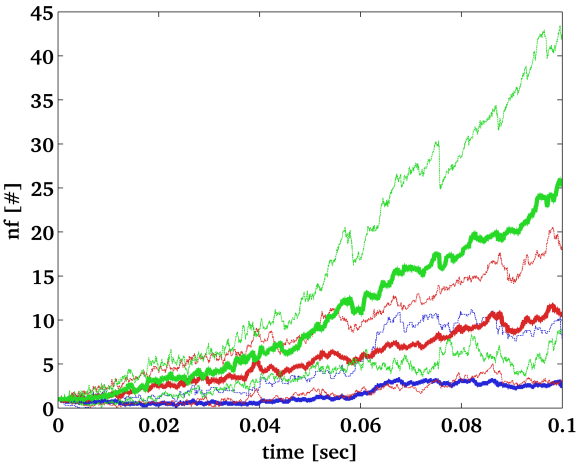

FIGURE 9. Number of GPIb-vWF bonds on platelet versus time. Green lines represent the mean (solid) ± standard deviation (dashed) values for $k_f^+ = 0.35/s$. Red lines and blue lines represent values for $k_f^+ = 0.25/s$ and $k_f^+ = 0.15/s$, respectively.

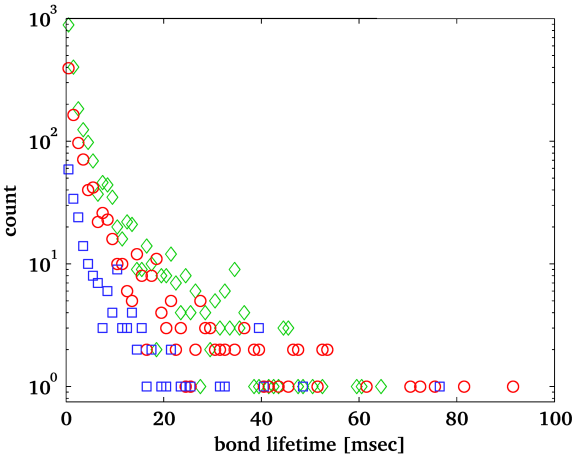

FIGURE 10. Histogram data of bond lifetimes. Blue squares, red circles, and green diamonds refer to cases with GPIb-vWF binding on rates of $k_f^+ = 0.15/s$, $k_f^+ = 0.25/s$, and $k_f^+ = 0.35/s$, respectively.

5. Platelet activation and $\alpha_{IIb}\beta_3$ bonds

During the platelet adhesion process a platelet may undergo a number of state changes which collectively are grouped under the umbrella of 'platelet activation'. The different changes start and are completed over different timescales ranging from subsecond to minutes [**37**]. A platelet may be stimulated to activate by multiple signaling systems, some of which interact synergistically. These include pathways turned on when platelets-secreted chemical agonists in the blood plasma (e.g. ADP

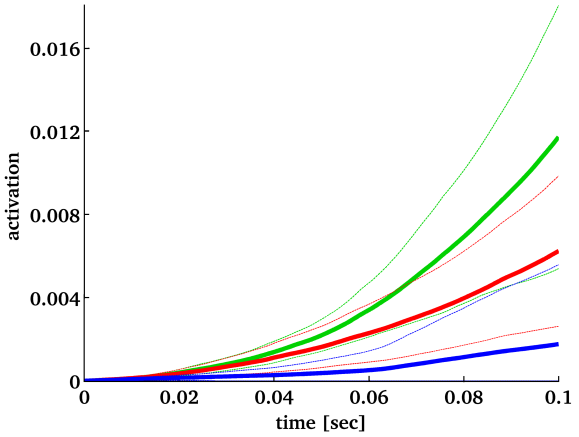

FIGURE 11. Platelet activation versus time. Green lines represent the mean (solid) ± standard deviation (dashed) values for $k_f^+ = 0.35/s$. Red lines and blue lines represent values for $k_f^+ = 0.25/s$ and $k_f^+ = 0.15/s$, respectively.

or thrombin) bind to their respective receptors on the platelet surface [**16**, **24**]. Activation responses also are stimulated by the changes in the cytoplasmic end of the platelet's adhesion receptors that occur when the receptors are bound to their respective extracellular ligands. In particular, the formation of GPIb-vWF adhesion bonds provides an activation stimulus [**43**]. Among the changes that the activating platelet undergoes is a change in the conformation of $\alpha_{IIb}\beta_3$ receptors from a low-affinity to high-affinity state [**8**]. This substantially increases their ability to participate in the platelet adhesion process.

5.1. Activation model. In the model, we greatly simplify the activation process by assuming that binding of GPIb receptors to vWF increases the platelet activation state and that the activation state in turn affects the rate of formation of bonds between $\alpha_{IIb}\beta_3$ and vessel surface molecules including vWF and fibrinogen. To this end we represent each platelet's activation state by a continuous variable A which ranges between 0 and 1. The value $A = 0$ corresponds to an unactivated platelet and $A = 1$ to a fully activated platelet. We assume that $A(t)$ obeys the kinetic equation

$$\frac{dA}{dt} = (k^A n_f^{tot})\,(1 - A) \tag{5.1}$$

where k^A is an activation rate constant and n_f^{tot} is the total number of GPIb-vWF bonds represented by all the platelet's links. We choose $k^A = 0.0016$/bond/s which implies that a platelet with one vWF-GPIb bond will reach half activation in 30 seconds.

Note that with this model $A(t)$ is monotone, increasing whenever GPIb-vWF bonds are present and remaining constant when they are not. Figure 11 shows the mean activation values for the platelets in the simulations described above.

5.2. $\alpha_{IIb}\beta_3$ bond dynamics. A platelet's value of A affects the binding parameters for its $\alpha_{IIb}\beta_3$ receptors. The unbinding rate is not affected and is assumed

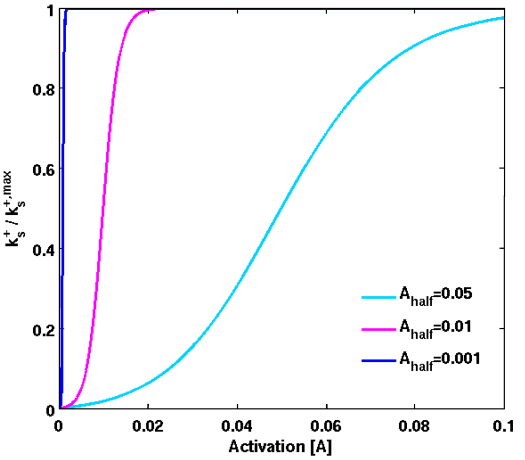

FIGURE 12. $\alpha_{IIb}\beta_3$ binding (Equation 5.4) on rate as a function of A. (note: $k_s^{+,\min} = 0$)

to follow the Bell model [**2**],

$$k_s^- = k_s^0 e^{\frac{y_s S_s (L - L_0)}{k_B T}} \tag{5.2}$$

with unloaded off rate $k_s^0 = 0.25$ s^{-1}, compliance parameter $y_s = 2.46$ nm, and spring stiffness $S_s = 12$ pN/nm. These parameters have been calculated from optical-trap force spectroscopy experiments between $\alpha_{IIb}\beta_3$ and fibrinogen molecules [**25**]. Because $y_s > 0$ in the Bell formula, these bonds act as slip bonds, i.e. they break at a rate that increases with the force acting on them.

For the simulations presented below we assume that the binding rate for $\alpha_{IIb}\beta_3$ bonds is

$$k_s^+(A)P(y)\,(n_{s,max} - n_s) \tag{5.3}$$

where the bond formation rate per available receptor $k_s^+(A)$ is given by

$$k_s^+(A) = \frac{A}{A + A_{\text{half}}^{A/A_{\text{half}}}} k_s^{+,\max} \tag{5.4}$$

Note that $k_s^+(A_{\text{half}})$ is half the maximum rate and smaller values of A_{half} produce sharper transitions (see Figure 12). In this paper we choose $A_{\text{half}} = 0.001$. In the previous simulations this value of A would have been reached between 30 and 40 msec according to Figure 11.

5.3. Simulation results. We perform two new sets of simulations with the same setup as before, but which now include the incorporated $\alpha_{IIb}\beta_3$ binding dynamics. Twelve simulations each are performed for $k_s^{+,max} = 0.1, 0.2/s$, with $k_f^+ = 0.25/s$. Each link now represents n_f GPIb-vWF bonds and n_s $\alpha_{IIb}\beta_3$ bonds. We create a link as before whenever a first n_f or n_s bond is formed. The probability of forming an n_f bond during timestep Δt is as above, and the probability of forming an n_s bond is

$$1 - e^{k_s^+(A)P(y)(n_{smax} - n_s)\Delta t}.$$

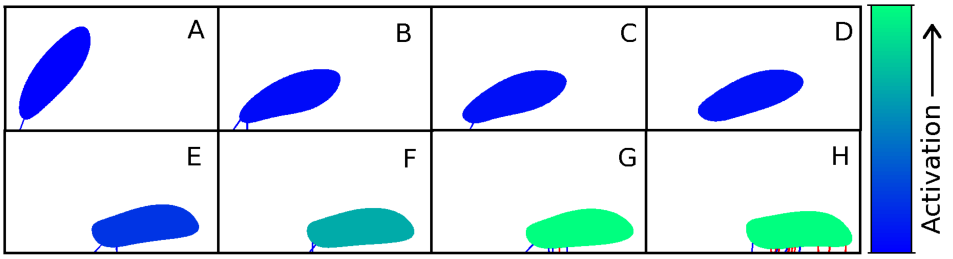

FIGURE 13. Snapshots in time of platelet adhesion. Time advances from (A) to (H). An unactivated platelet initially binds to the vessel wall with a GPIb-vWF bond (A). It translates along the wall via other transient GPIb-vWF bonds (blue lines) while increasing its activation status (B)-(F). Once sufficiently active, it begins to form $\alpha_{IIb}\beta_3$ integrin bonds (red lines) (G) and firmly adheres to the vessel wall (H). Activation color scale ranges from a value of 0.0 (blue) to 0.001 (green).

The force a link generates is modified to become

$$F = (n_f S_f + n_s S_s)(L - L_0)$$

still in the direction given by the link.

Starting from an initial condition with one GPIb-vWF bond and the platelet in a configuration perpendicular to the wall, we observe similar behaviors as before but the platelet now firmly adheres when the $\alpha_{IIb}\beta_3$ bonds start forming. The mean platelet velocities tangential to the wall after the platelet reaches an activation level of 0.001 (the level to achieve half of the $k_s^{+,max}$) are -0.04 nm/s for $k_s^{+,max} = 0.1$ (indicating slight retraction) and 0.4 nm/s for $k_s^{+,max} = 0.2$. These compare to a mean platelet center of mass velocity of 9.3 μm/s when only GPIb-vWF bonds are included in the calculations. Thus, the $\alpha_{IIb}\beta_3$-mediated bonds are capable of immobilizing the platelet on the vessel wall. During the 100 msec of simulation a platelet makes a mean number of 34 and 86 $\alpha_{IIb}\beta_3$ bonds for $k_s^+ = 0.1\ s^{-1}$ and $k_s^+ = 0.2\ s^{-1}$, respectively. Without the $\alpha_{IIb}\beta_3$ bonds we observe a mean of ≈ 86 GPIb-vWF bonds during 100 msec of simulation. With the $\alpha_{IIb}\beta_3$ bond dynamics present we observe a decrease of $\approx$ 26 GPIb-vWF bonds for both cases. The explanation for this behavior is that the bonds tend to be shorter when the $\alpha_{IIb}\beta_3$ bond forces are included, and the shorter bond length can increase the unbinding if GPIb-vWF bonds because of their catch-bond mechanism.

5.4. Platelet-platelet cohesion bond model. GPIb-vWF bonds and bonds involving vWF or fibrinogen bound to $\alpha_{IIb}\beta_3$ receptors on two platelets are important in platelet cohesion and thus in aggregate formation. Here we report preliminary results of work to extend the binding models described above to platelet cohesion. The simulations involve two platelets, one of which is activated and firmly held in place near the vessel wall, and the other of which is not activated and has a single GPIb-vWF bond with the immobilized platelet. For these preliminary studies, we assume that the surface densities of vWF and fibrinogen bound to the surface of the immobilized platelet are the same as that on the vessel wall, so that the binding kinetic parameters for cohesion are the same as we used for adhesion.

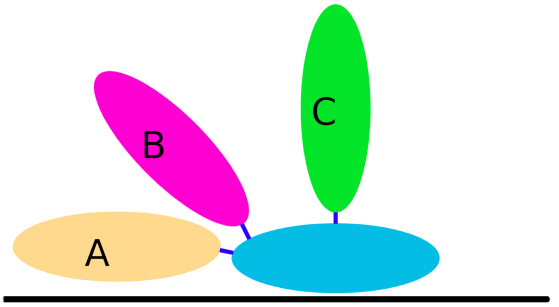

FIGURE 14. Initial configurations for a platelet adhering to another platelet immobilized on the vessel wall. Six simulations are computed for each configuration. The blue lines represent a link with one GPIb-vWF bond.

Different simulations are begun with the mobile platelet attached to the immobilized one at different locations and with different orientations. See Figure 14. For these simulations, the shear rate is 2000 s^{-1}, $k_f^+ = 0.25/s$, and $k_s^{+,max} = 0.2/s$. The mobile platelets may form additional bonds with the immobilized one in addition to bonds it forms with the vessel wall.

Figure 15 shows snapshots from two simulations with the mobile platelet initially in different locations relative to the immobilized one. The top sequence shows that the platelet which began upstream of the immobilized one moved slowly toward and began to slide over the immobilized platelet. Over the course of this motion, it formed numerous GPIb-vWF bonds with the other platelet as well as some with the vessel wall. These provided an activation stimulus sufficient to bring the stronger and longer-lived $\alpha_{IIb}\beta_3$-mediated bonds into play.

In the bottom sequence, the mobile platelet tumbles over the immobilized one transiently forming GPIb-vWF bonds with it. Activation is slower in this case, the number of GPIb-vWF bonds decreases with time, and at the end of the simulation, the mobile platelet is attached only to the immobilized platelet's downstream end. In a simulation with a mobile platelet positioned as in Figure 15 case B, the behavior was very similar.

6. Discussion

We have developed a mesoscale model of platelet binding processes. It treats bond formation and breaking stochastically with realistic kinetics without requiring that we track the evolving state of each of the thousands of individual binding receptors as is done in some other work. We have included these models in an immersed-boundary-based framework to simulate platelet adhesion and cohesion. This is a significant improvement in the way binding dynamics are handled compared to our earlier computational models [**13**]. The use of IBAMR has allowed us to take advantage of adaptive mesh refinement to better resolve fluid motion in the vicinity of aggregating platelets. We note that the extensions to IBAMR made for this project to allow dynamic link formation and breaking may find use in other applications.

The motion of platelets in the simulations with only GPIb-vWF bonds display the stop-start behavior that has been seen in experimental studies [**4**]. In examining this motion, we see that relatively few of the adhesion bonds are long-lived. This is a consequence of the catch-bond nature of the GPIb-vWF bond dynamics. The many short-lived bonds seem to have a stabilizing effect in that platelets detached from the vessel wall less often in simulations with higher k_f^+ values and faster bond turnover. The short-lived bonds also increase the rate of platelet activation which promotes $\alpha_{IIb}\beta_3$-mediated binding.

We use a simple first order equation (Equation 5.1) to model platelet activation in response to GPIb-vWF binding. Its dynamics allow us to define a timescale for activation and for events which occur during the activation process. This is in contrast to our earlier models which assumed that activation occurs instantaneously [**11**] after stimulus. In our new model, the platelet activation state is tracked as a continuous variable that captures the history of the various stages of activation. Currently only GPIb-vWF bonds govern the rate of activation and over the short timescale of the simulations presented here the value of the activation state is low (< 0.02). The purpose of activation here is solely to control $\alpha_{IIb}\beta_3$ integrin binding. However, this model can be expanded in the future to encompass more platelet activators (ADP, membrane shear, different bonds) and more responses (release of granule contents, shape change, pseudopodia extension) that will occur at larger activation values.

When we add $\alpha_{IIb}\beta_3$-mediated binding, platelets can become firmly-adherent to the vessel wall. The platelets undergo a transient stop-start motion from the GPIb-vWF binding while they increase their activation levels. Once the activation level is sufficiently high and $\alpha_{IIb}\beta_3$-mediated bonds form, the platelet firmly adheres to the vessel wall. Our reported distances and times until the occurrence of firm adhesion should not be taken to quantitatively predict experimental results. This is because of great uncertainty in the bond formation rate data and the 2D nature

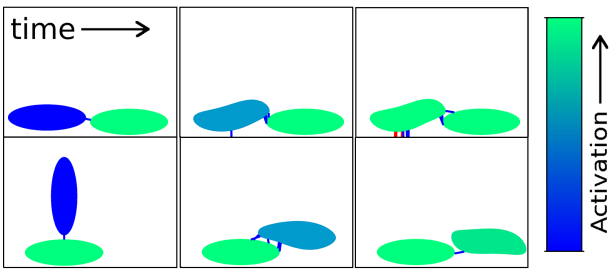

FIGURE 15. Snapshots of a platelet attaching to an immobilized platelet from two different initial configurations. Activation color scale ranges from a value of 0.0 (blue) to 0.001 (green). The top shows the platelet sliding up over the immobilized platelet and making GPIb bonds with it and the vessel wall while activating. This leads to the formation of $\alpha_{IIb}\beta_3$ bonds. The bottom shows the platelet tumbling over the immobilized platelet making GPIB bonds and increasing its activation status but not making any $\alpha_{IIb}\beta_3$ bonds. At the end of the simulation it is bound to the downstream edge of the immobilized platelet.

of these simulations which can have a strong influence on the fluid forces exerted on the platelets and its bonds with the vessel wall. We expect that further work in 3D will allow us to place constraints on the values of the bond formation rates and to provide quantitative predictions about the distances from the time of first adhesion until the platelet is stably adhered.

We were able to report on the forces required to immobilize a 3D platelet. Arterioles in the body operate at shear rates of 1000 to 2000 s^{-1}. At these physiological shear rates only 70 to 122 pN of force is required to hold a platelet in place. This is the same order of magnitude as the rupture force for $\alpha_{IIb}\beta_3$ bonds [**26**], indicating that very few bonds, perhaps only one, may be required at any given time to immobilize a platelet to the vessel wall. However, once additional platelets bind to such a platelet, the situation changes and the force required may increase or decrease depending on the configuration of the platelets and bonds.

In this study, the two-layer approach to model platelet allows them to deform. In the 3D immobilization force simulations, this deformation is less than 1% and should not have affected the forces measured. for the longer and more numerous 2D simulations, more platelet deformation is allowed to lessen the computational cost. The deformation does not impact the qualitative results reported from these simulations.

In this work, we have taken a significant step toward including recent information about the complex force-dependent kinetics of platelet-surface and platelet-platelet binding and unbinding in our IB-based model of platelet aggregation. The models still have limitations. A prominent one, pertinent to platelet cohesion, is that explicit consideration of the bridging molecules (vWF, fibrinogen) is not included. (See [**30**] for a study in which the kinetics of soluble vWF binding to a platelet surface was considered.) Furthermore, the concentration of these molecules in the vicinity of a growing aggregate is expected to undergo large dynamic changes as a consequence of platelet secretion, in the case of vWF, and, in the case of fibrinogen, of competitive consumption to form a fibrin gel once the coagulation cascade has fully come into play [**22**]. Also, we have shown in previous work [**15**] that the times that have elapsed since their activation for two platelets that come into close proximity may strongly influence their ability to cohere. Models that include the bridging molecules are under development.

7. Acknowledgements

This work was supported by NIH grant 1R01GM090203-01, NSF grant DMS-1160432, and an allocation for computer resources at the University of Utah Center for High Performance Computing (CHPC). IBAMR was developed through the support of NSF Software Infrastructure for Sustained Innovation award (NSF OCI 1047734). The authors are grateful to Jim Keener, Mike Kirby, Wendy Thomas, and Vince Turitto for helpful discussions during the course of this work.

References

[1] M. Auton, C. Zhu, and M.A. Cruz, *The mechanism of vWF-mediated platelet GPIbα binding*, Biophys J **99** (2010), 1192–1201.
[2] G.I. Bell, *Models for the specific adhesion of cells to cells*, Science **200** (1978), 618–627.
[3] D.K. Brunk and D.A. Hammer, *Quantifying rolling adhesion with a cell-free assay: E-selectin and its carbohydrate ligands.*, Biophys J. **72** (1997), 2820–33.

[4] L.A. Coburn, V.S. Damaraju, S. Dozic, S.G. Eskin, M.A. Cruz, and L.V. McIntire, *GPIbα-vWF rolling under shear stress shows differences between type 2B and 2M von Willebrand disease*, Biophys J **100** (2011), 304–312.

[5] L. M. Crowl and A. L. Fogelson, *Analysis of mechanisms for platelet near-wall excess under arterial blood flow conditions*, J. Fluid Mech. **676** (2011), 348–375, DOI 10.1017/jfm.2011.54. MR2804454 (2012e:92024)

[6] L. M. Crowl and A. L. Fogelson, *Computational model of whole blood exhibiting lateral platelet motion induced by red blood cells*, Int. J. Numer. Methods Biomed. Eng. **26** (2010), no. 3-4, 471–487, DOI 10.1002/cnm.1274. MR2655874

[7] T.A. Doggett, G. Girdhar, A. Lawshe, D.W. Schmidtke, I.J. Laurenzi, S.L. Diamond, and T.G. Diacovo, *Selectin-like kinetics and biomechanics promote rapid platelet adhesion in flow: The GPIbα-vWF tether bond*, Biophysical Journal **83** (2002), 184–205.

[8] X. Du, *The platelet glyoprotein IIb-IIIa complex (integrin $\alpha_{IIb}\beta_3$)*, Platelets, Thrombosis and the Vessel Wall (M.C. Berndt, ed.), Advances in Vascular Biology, vol. 6, 2000, pp. 83–101.

[9] E.C. Eckstein, A.W. Tilles, and F.J. Millero, *Conditions for the occurence of large near-wall excesses of small particles during blood flow*, Microvasc Res **36** (1988), 31–39.

[10] A.L. Fogelson, *A mathematical model and numerical method for studying platelet adhesion and aggregation during blood clotting*, J. Comput. Phys. **56** (1984), no. 1, 111–134, DOI 10.1016/0021-9991(84)90086-X. MR760745 (86a:92013)

[11] A.L. Fogelson, *Cell-based models of blood clotting*, pp. 243–269, Birkhäuser Verlag, 2007.

[12] A.L. Fogelson and R.D. Guy, *Immersed-boundary-type models of intravascular platelet aggregation*, Comput. Methods Appl. Mech. Engrg. **197** (2008), no. 25-28, 2087–2104, DOI 10.1016/j.cma.2007.06.030. MR2412813 (2009f:74024)

[13] A.L. Fogelson, A. Kuharsky, and H. Yu, *Computational modeling of blood clotting: Coagulation and three-dimensional platelet aggregation*, Polymer and Cell Dynamics: Multicsale Modeling and Numerical Simulations (W. Alt, M. Chaplain, M. Griebel, and J. Lenz, eds.), Birkhaeuser-Verlag, Basel, 2003, pp. 145–154.

[14] B.E. Griffith, X. Lou, D.M. McQueen, and C.S. Peskin, *Simulating the fluid dynamics of natural and prosthetic heart valves using the immersed boundary method*, Int J Appl Mech **1** (2009), 137–177.

[15] R. D. Guy and A. L. Fogelson, *Probabilistic modeling of platelet aggregation: effects of activation time and receptor occupancy*, J. Theoret. Biol. **219** (2002), no. 1, 33–53, DOI 10.1016/S0022-5193(02)93106-1. MR2043349

[16] M. Holinstat, A.M. Preininger, S.B. Milne, W.J. Hudson, H.A. Brown, and H.E. Hamm, *Irreversible platelet activation requires protease-activated receptor 1-mediated signaling to phosphatidylinositol phosphates*, Molecular Pharmacology **76** (2009), no. 2, 301–313.

[17] G. Interlandi and W. Thomas, *The catch bond mechanism between von Willebrand Factor and platelet surface receptors investigated by molecular dynamics simulations*, Proteins **78** (2010), 2506–2522.

[18] S.P. Jackson, *The growing complexity of platelet aggregation*, Blood **109** (2007), no. 12, 5087–5095.

[19] S.P. Jackson, W.S. Nesbitt, and E. Westein, *Dynamics of platelet thrombus formation*, J Thromb Haemost **7** (2009), 17–20.

[20] S. Jadhav, C.D. Eggleton, and K. Konstantopoulos, *A 3-d computational model predicts that cell deformation affects selectin-mediated leukocyte rolling*, Biophys J **88** (2005), 96–104.

[21] A. Kasirir-Friede, M.R. Cozzi, M. Mazzucato, L. De Marco, Z.M. Ruggeri, and S.J. Shattil, *Signaling through GP Ib-IX-V activates $\alpha_{IIb}\beta_3$ independently of other receptors*, Blood **103** (2004), 3403–3411.

[22] A.L. Kuharsky and A.L. Fogelson, *Surface-mediated control of blood coagulation: The role of binding site densities and platelet deposition*, Biophys J **80** (2001), 1050–1074.

[23] D.A. Lauffenburger and J.L. Linderman, *Receptors: models for binding, trafficking, and signaling*, Oxford University Press, New York, 1993.

[24] Z. Li, M.K. Delaney, K.A. O'Brien, and X. Du, *Signaling during platelet adhesion and activation*, Arteriosclerosis, Thrombosis, and Vascular Biology **30** (2010), no. 12, 2341–2349.

[25] R.I. Litvinov, V. Barsegov, A.J. Schissler, J.S. Bennett, J.W. Weisel, and H. Shuman, *Dissociation of bimolecular αIIbβ3-fibrinogen complex under a constant tensile force*, Biophys J **100** (2011), 165–173.

[26] R.I. Litvinov, J.S. Bennett, J.W. Weisel, and H. Shuman, *Multi-step fibrinogen binding to the integrin $\alpha IIb\beta 3$ detected using force spectroscopy*, Biophys J **89** (2005), 2824–2834.
[27] M.J. Maxwell, S.M. Dopheide, S.J. Turner, and S.P. Jackson, *Shear induces a unique series of morphological changes in translocating platelets: effects of morphology on translocation dynamics*, Arterioscler. Thromb. Vasc. Biol. **26** (2006), 663–669.
[28] N.A. Mody and M.R. King, *Three-dimensional simulations of a platelet-shaped spheroid near a wall in shear flow*, Physics of Fluids **17** (2005).
[29] ———, *Platelet adhesive dynamics. part I: characterization of platelet hydrodynamic collisions and wall effects*, Biophys J **95** (2008), 2539–2555.
[30] ———, *Platelet adhesive dynamics. part II: high shear-induced transient aggregation via GPIbα-vWF-GPIbα bridging*, Biophys J **95** (2008), 2556–2574.
[31] Aarts P.A.M.M., P. Steendjik, J.J. Sixma, and R.M. Heethaar, *Fluid shear as a possible mechanism for platelet diffusivity in flowing blood*, J. Biomechanics **19** (1986), 799–805.
[32] Y.V. Pereverzev, O.V. Prezhdo, M. Forero, E.V. Sokurenko, and WE Thomas, *The two-pathway model for the catch-slip transition in biological adhesion.*, Biophys J. **89** (2005), 1446–54.
[33] C. S. Peskin, *The immersed boundary method*, Acta Numer. **11** (2002), 479–517, DOI 10.1017/S0962492902000077. MR2009378 (2004h:74029)
[34] C. Pozrikidis, *Flipping of an adherent blood platelet over a substrate*, J. Fluid Mech. **568** (2006), 161–172, DOI 10.1017/S002211200600156X. MR2273388
[35] T. Riedel, J. Suttnar, E. Brynda, M. Houska, L. Medved, and J.E. Dyr, *Fibrinopeptides a and b release in the process of surface fibrin formation*, Blood **117** (2011), no. 5, 1700–1706.
[36] Z.M. Ruggeri and C.G. Mendolicchio, *Adhesion mechanics in platelet function*, Circulation Research **100** (2007), 1673–1685.
[37] J.G. Schaller and U Simon Kaempfer, *Human blood plasma proteins: structure and function*, Wiley, Hoboken, NJ, 2008.
[38] T. Skorczewski, L.M. Crowl, and A.L. Fogelson, *Platelet motion near a vessel wall or thrombus surface in 2D whole blood simulations*, Biophys J **104** (2013), 1764–1772.
[39] H. Slayter, J. Loscalzo, P. Bockenstedt, and R.I. Handin, *Native conformation of human von Willebrand protein*, J. Biol. Chem. **260** (1985), 8559–8563.
[40] A.W. Tilles and E.C. Eckstein, *The near-wall excess of platelet-sized particles in blood flow: its dependence on hematocrit and wall shear rate*, Microvasc Res **33** (1987), 211–223.
[41] T. Yago, J. Lou, T. Wu, J. Yang, J.J. Miner, L. Coburn, J.A. Lopez, M.A. Cruz, J.F. Dong, L.V. McIntire, R.P. McEver, and C Zhu, *Platelet glycoprotein Ibα forms catch bonds with human WT vWF but not with type 2B von Willebrand disease vWF.*, J Clin Invest. **118** (2008), 3195–207.
[42] T. Yago, J. Wu, C.D. Wey, A.G. Klopocki, C. Zhu, and R.P. McEver, *Catch bonds govern adhesion through L-selectin at threshold shear*, Journal of Cell Biology **166** (2004), 913–923.
[43] H. Yin, A. Stojanovic, N. Hay, and X. Du, *The role of Akt in the signaling pathway of the glycoprotein Ib-IX-induced platelet activation*, Blood **111** (2008), no. 2, 658–665.
[44] H. Zhao, E.S.G. Shaqfeh, and V. Narsimhan, *Shear-induced particle migration and margination in a cellular suspension*, Physics of Fluids **24** (2012).

Department of Mathematics, University of Utah
E-mail address: tskorc@math.utah.edu

Leon H. Charney Division of Cardiology, Department of Medicine, New York University School of Medicine
E-mail address: boyce.griffith@nyumc.org

Department of Mathematics, Courant Institute of Mathematical Sciences, New York University
E-mail address: griffith.cims.nyu.edu

Department of Mathematics, University of North Carolina at Chapel Hill
E-mail address: boyceg@email.unc.edu

Department of Mathematics and Bioengineering, University of Utah
E-mail address: fogelson@math.utah.edu